Spectral response modeling and analysis of p–n–p $In_{0.53}Ga_{0.47}As$/InP HPTs*

Jun Chen(陈俊)† and Jiabing Lv(吕加兵)

School of Electronic and Information Engineering, Soochow University, Suzhou 215006, *China*

(Received 22 February 2016; revised manuscript received 29 April 2016; published online 19 July 2016)

We report our results on the modeling of the spectral response of the near-infrared (NIR) lattice-matched p–n–p $In_{0.53}Ga_{0.47}As$/InP heterojunction phototransistors (HPTs). The spectral response model is developed from the solution of the steady state continuity equations that dominate the excess optically generated minority-carriers in the active regions of the HPTs with accurate boundary conditions. In addition, a detailed optical-power absorption profile is constructed for the device modeling. The calculated responsivity is in good agreement with the measured one for the incident radiation at 980 nm, 1310 nm, and 1550 nm. Furthermore, the variation in the responsivity of the device with the base region width is analyzed.

Keywords: spectral response, near-infrared heterojunction phototransistors, responsivity

PACS: 72.80.Ey, 73.40.Kp, 73.61.Ey, 78.20.Bh **DOI:** 10.1088/1674-1056/25/9/097202

1. Introduction

Development of photodetectors with high sensitivity, high speed, and low power consumption has been a main goal in device research for optical communication applications. Metal–semiconductor–metal (MSM) and p–i–n photodetectors can provide high speed, low noise operation but no internal gain.[1–4] Avalanche photodiodes (APDs) can achieve high sensitivity due to the large internal gain, however, they need high operation voltages.[5] It is therefore expected that heterojunction phototransistors (HPTs) can provide an exciting alternative to p–i–n photodetectors or APDs for the optical communication application. An HPT basically is a heterojunction bipolar transistor with a light-sensitive collector and base region; the incoming light is absorbed in the narrow bandgap collector and base region, producing electron–hole pairs. The amplification process is the same as that in a transistor, except that the base–emitter forward bias is provided by the optical absorption process rather than a metal contact.[6,7]

Spectral response is a key performance parameter for many photoelectric devices. Even though many reports involving spectral response models have emerged recently for photodiodes,[8–10] analytical models for HPTs are still rather limited. Chand *et al.* formulated the expressions for the flux-dependent current,[11] but the boundary conditions were taken from the p–i–n photodetectors, which were not effective for the HPTs, in addition, no experimental data were used to verify the theory they proposed. Several others tried to predict the spectral response of HPTs, but the absorption coefficients in those studies were taken as unity for all the layers in the HPTs, which may not be the case for every detector.[12–14] Khan *et al.* optimized the necessary analytical expressions of the spectral response model using the doping-dependent collection efficency with the incident light radiated at the base region directly.[15] However, according to the theory of Chand,[11] the diffusion current coming from the neutral portion sub-collector should be taken into consideration in calculating the depleted-collector current, which was neglected by Khan owing to the relatively small diffusion coefficients of the minority-carrier holes in the n-type sub-collecter. Furthermore, there are many integrated devices currently employing HPTs with a floating base such as HPTs/OLEDs optical up-converter[16,17] and HPTs/LDs,[18,19] which require the light radiated from the emitter of the HPTs. Moreover, in the optical up-converter, the p–n–p InGaAs/InP HPTs are usually chosen to be integrated with the anode of OLEDs. Thus, the establishment of the spectral response model for the p–n–p HPTs is necessary.

In this paper, we present a back illuminated p–n–p $In_{0.53}Ga_{0.47}As$/InP HPT along with a corresponding spectral response model. The epitaxial layer structure of this device consists of a p-type InP layer as emitter, a thin n-type $In_{0.53}Ga_{0.47}As$ layer as base, and a p-type $In_{0.53}Ga_{0.47}As$ layer as collector. Unlike the structure of Khan *et al.*,[15,20,21] the emitter/base junction and the collector/sub-collector junction in our model are neither exposed to the air nor contacted to the metal. So not only the photo-generated minority carriers but

*Project supported by the National Natural Science Foundation of China (Grant No. 61307044), the National Basic Research Program of China (Grant No. 2012CB619200), the Natural Science Foundation of Jiangsu Province, China (Grant No. BK20130321), the Research Fund for the Doctoral Program of Higher Education of China (Grant No. 20133201120009), the Open Project of Key Laboratory of Infrared Imaging Materials and Detectors, Chinese Academy of Sciences (IIMDKFJJ-15-06), the Scientific Research Foundation for the Returned Overseas Chinese Scholars, Ministry of Education of China, and the Research Innovation Program for College Graduates of Jiangsu Province, China (Grant No. SJLX15-0600).

†Corresponding author. E-mail: junchen@suda.edu.cn

© 2016 Chinese Physical Society and IOP Publishing Ltd

also the thermal equilibrium minority carriers electrons (holes) in these regions should be taken into account in the boundary conditions of the spectral response model. The main aim of this study is to determine the spectral response model for the p–n–p HPT which has a perfect agreement with the measurements. Moreover, a nearly proportional relationship between the response and the base width is found in this paper.

2. Device structure

The $In_{0.53}Ga_{0.47}As$/InP HPT was grown by metal-organic chemical vapor deposition (MOCVD) on a semi-insulated InP substrate. The epitaxy structure is as follows: 500 nm InP emitter contact (p^+, 1×10^{18} cm^{-3}), 300 nm InP emitter layer (p, 5×10^{17} cm^{-3}), 100 nm InGaAs base layer (n^+, 1×10^{18} cm^{-3}), 1 μm InGaAs collector layer (p, 5×10^{17} cm^{-3}). The HPT was capped with a 500 nm InGaAs contact layer (p^+, 1×10^{18} cm^{-3}). The first step of the device fabrication was to pattern and etch square mesas (1 mm×1 mm). The solution of H_2SO_4:H_2O_2:H_2O (1:8:160) was used to etch the InGaAs layer (∼1.6 μm thick), and the solution of H_3PO_4:HCl (10:1) was used to etch part of the p-InP layer (∼ 0.5 μm thick) to complete the square mesas (Fig. 1). Subsequently, metal (Ti/Pt/Au) contacts were deposited on the top and bottom of the device by electron beam evaporation. The spectral response measurements were carried out using a BOMEM spectrometer over 900–1700 nm.

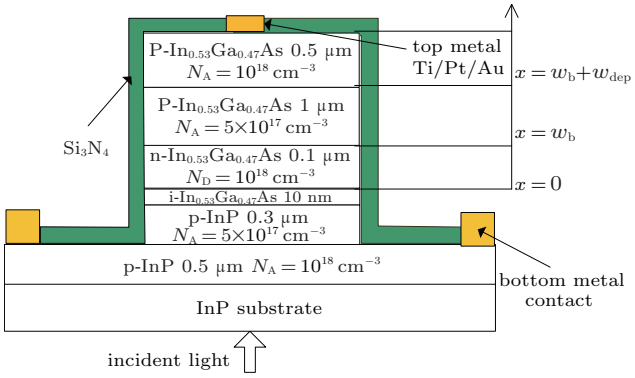


Fig. 1. (color online) Schematic cross section of the $In_{0.53}Ga_{0.47}As$/InP HPT. Note that the top and bottom metal contacts consist of 25 nm Ti, 55 nm Pt, and 120 nm Au.

3. Spectral response modeling

When the p–n–p HPT is exposed to the incoming near-infrared (NIR) light, electron–hole pairs will be generated in the base, depleted-collector, and sub-collector regions. These electrons and holes will be driven to the contrary directions (electrons drifting towards the n-type base region and holes to the p-type sub-collector). The photo-generated electrons will accumulate in the base region due to a large potential barrier in the conduction band at the base–emitter heterojunction until they recombine with the injected holes from the emitter. Thus a large amount of holes inject from the emitter into the base to maintain the charge-neutrality condition in the base layer, leading to a large hole current.

The spectral response model is based on the steady state continuity equations with suitable boundary conditions. The distributions of minority-carriers (electrons and holes) at the low-injection state in the base and sub-collector regions respectively obey

$$D_p\frac{\mathrm{d}^2p_n}{\mathrm{d}x^2}-\frac{p_n-p_{n0}}{\tau_p}+\varphi_\mathrm{b}\alpha_\mathrm{b}\exp(-\alpha_\mathrm{b}x)=0, \tag{1}$$

$$D_n\frac{\mathrm{d}^2n_p}{\mathrm{d}x^2}-\frac{n_p-n_{p0}}{\tau_n}+\varphi_\mathrm{c}\alpha_\mathrm{c}\exp(-\alpha_\mathrm{c}x)=0, \tag{2}$$

where p_n (n_p) and p_{n0} (n_{p0}) are the total and the equilibrium hole (electron) concentrations in the base (sub-collector), D_p (D_n) and τ_p (τ_n) are the diffusion coefficient and the lifetime of the minority-carrier holes (electrons) in the n^+-InGaAs base (p^+-InGaAs sub-collector) layer, respectively, α_b and α_c are the optical absorption coefficients of the base and the sub-collector layers, respectively, and φ_b and φ_c are the incident flux densities at the emitter/base ($x=0$) and the depleted-collector/sub-collector ($x=w_\mathrm{b}+w_\mathrm{dep}$) junctions, respectively. The boundary conditions for the base region are modelled as[21]

$$p_n(x=0)=\frac{\varphi_\mathrm{b}}{s_p}+p_{n0}, \tag{3}$$

$$p_n(x=w_\mathrm{b})=\frac{\varphi_\mathrm{b}}{s_p}\exp(-\alpha_\mathrm{b}w_\mathrm{b})+p_{n0}, \tag{4}$$

where s_p is the surface recombination velocity of holes in the n^+-InGaAs base. Using Eqs. (2)–(4), the hole distribution in the base region and the hole current at the base/depleted-collector junction $I_{x=w_\mathrm{b}}$ are given respectively as

$$\begin{aligned}p_n=\;&p_{n0}-\frac{\tau_p\varphi_\mathrm{b}\alpha_\mathrm{b}}{L_p^2\alpha_\mathrm{b}^2-1}\mathrm{e}^{-\alpha_\mathrm{b}x}\\&+\left\{\frac{\varphi_\mathrm{b}}{s_p}\frac{\mathrm{e}^{-\alpha_\mathrm{b}w_\mathrm{b}}-\mathrm{e}^{-w_\mathrm{b}/L_p}}{2\sinh(w_\mathrm{b}/L_p)}\right.\\&\left.+\frac{\tau_p\varphi_\mathrm{b}\alpha_\mathrm{b}}{L_p^2\alpha_\mathrm{b}^2-1}\frac{\mathrm{e}^{-\alpha_\mathrm{b}w_\mathrm{b}}-\mathrm{e}^{-w_\mathrm{b}/L_p}}{2\sinh(w_\mathrm{b}/L_p)}\right\}\mathrm{e}^{x/L_P}\\&+\left\{\left[\frac{\varphi_\mathrm{b}}{s_n}\frac{\mathrm{e}^{w_\mathrm{b}/L_p}-\mathrm{e}^{-\alpha_\mathrm{b}w_\mathrm{b}}}{2\sinh(w_\mathrm{b}/L_p)}\right]\right.\\&\left.-\frac{\tau_p\varphi_\mathrm{b}\alpha_\mathrm{b}}{L_p^2\alpha_\mathrm{b}^2-1}\frac{\mathrm{e}^{-\alpha_\mathrm{b}w_\mathrm{b}}-\mathrm{e}^{w_\mathrm{b}/L_p}}{2\sinh(w_\mathrm{b}/L_p)}\right\}\mathrm{e}^{-x/L_P},\end{aligned} \tag{5}$$

$$\begin{aligned}I_{x=w_\mathrm{b}}=\;&\frac{qD_pA}{L_p\sinh(w_\mathrm{b}/L_p)}\left\{\frac{\varphi_\mathrm{b}}{s_p}\left[\cosh\left(\frac{w_p}{L_p}\right)\mathrm{e}^{-\alpha_\mathrm{b}w_\mathrm{b}}-1\right]\right.\\&+\frac{\tau_p\varphi_\mathrm{b}\alpha_\mathrm{b}}{L_p^2\alpha_\mathrm{b}^2-1}\left[a_\mathrm{b}L_p\sinh\left(\frac{w_\mathrm{b}}{L_p}\right)\mathrm{e}^{-\alpha_\mathrm{b}w_\mathrm{b}}\right.\\&\left.\left.+\cosh\left(\frac{w_\mathrm{b}}{L_p}\right)\mathrm{e}^{-\alpha_\mathrm{b}w_\mathrm{b}}-1\right]\right\},\end{aligned} \tag{6}$$

where q is the charge of an electron, A is the area of the photosensitive part of the HPT, and $L_p = \sqrt{D_p \tau_p}$ is the minority-hole diffusion length in the base region. The boundary conditions for the sub-collector region are modeled as

$$n_p(x = w_b + w_{dep}) = \frac{\varphi_c}{s_n} + n_{p0}, \tag{7}$$

$$n_p(x = w_b + w_{dep} + w_c) = \frac{\varphi_c}{s_n} \exp(-\alpha_c w_c) + n_{p0}. \tag{8}$$

The electron current in the sub-collector region $I_{x=w_b+w_{dep}+w_c}$ can be similarly derived as

$$\begin{aligned} & I_{x=w_b+w_{dep}+w_c} \\ &= -\frac{qD_nA}{L_n \sinh(w_c/L_n)} \left\{ \frac{\varphi_c}{s_n} \left[\cosh\left(\frac{w_c}{L_n}\right) e^{-\alpha_c w_c} - 1 \right] \right. \\ &+ \frac{\tau_n \varphi_c \alpha_c}{L_n^2 \alpha_c^2 - 1} \left[\alpha_c L_n \sinh\left(\frac{w_c}{L_n}\right) e^{-\alpha_c w_c} \right. \\ &\left. \left. + \cosh\left(\frac{w_c}{L_n}\right) e^{-\alpha_c w_c} - 1 \right] \right\}. \end{aligned} \tag{9}$$

The current in the depleted-collector layer I_{dr} consists of photo-generated current I_{ph} and diffusion current $I_{x=w_b+w_{dep}}$. The former is owing to the optical-flux absorption, the latter is the result of the electrons diffusion from the neutral portion, which are respectively given as

$$\begin{aligned} I_{ph} &= qA \int_{w_b}^{w_b+w_{dep}} \varphi_{dep} \alpha_{dep} \exp(-\alpha_{dep} x)\, dx \\ &= qA\varphi_{dep} \left[1 - \exp(-\alpha_{dep} w_{dep}) \right], \end{aligned} \tag{10}$$

$$\begin{aligned} & I_{x=w_b+w_{dep}} \\ &= -\frac{qD_nA}{L_n \sinh(w_c/L_n)} \left\{ \frac{\varphi_c}{s_n} \left[e^{-\alpha_c w_c} - \cosh\left(\frac{w_c}{L_n}\right) \right] \right. \\ &\left. + \frac{\tau_n \varphi_c \alpha_c}{L_n^2 \alpha_c^2 - 1} \left[\alpha_c L_n \sinh\left(\frac{w_c}{L_n}\right) + e^{-\alpha_c w_c} - \cosh\left(\frac{w_c}{L_n}\right) \right] \right\}, \end{aligned} \tag{11}$$

where φ_{dep} is the incident flux density at the base-collector ($x = w_b$) junction, and α_{dep} is the optical absorption coefficient in the depletion region.

4. Results and discussion

The optical-flux profiles of the active regions in the p–n–p $In_{0.53}Ga_{0.47}As$/InP HPT at 980 nm, 1310 nm, and 1550 nm are given numerically in Fig. 2 with the incident light power of 1 mV, which are modeled by

$$\varphi(x) = \varphi_0 \left[1 - \frac{(n_{InP} - n_0)^2}{(n_{InP} + n_0)^2} \right] \left[1 - \frac{(n_{InGaAs} - n_{InP})^2}{(n_{InGaAs} + n_{InP})^2} \right] \begin{cases} e^{-\alpha_b x}, & 0 \le x \le w_b, \\ (1 - e^{-\alpha_b w_b})\, e^{-\alpha_{dep} x}, & w_b \le x \le w_b + w_{dep}, \\ (1 - e^{-\alpha_b w_b})\, e^{-\alpha_{dep} w_{dep}}\, e^{-\alpha_c x}, & w_b + w_{dep} \le x \le w_b + w_{dep} + w_c, \end{cases} \tag{12}$$

where $n_0 = 1$, $n_{InP} = 3.1$, and $n_{InGaAs} = 3.9$ are the refractive indices of air, InP, and InGaAs, respectively,[22] and φ_0 is the flux density of the input light. Due to the absence of anti-reflection coatings, the input optical flux in our model will experience Fresnel reflection at the air/InP and InP/InGaAs interfaces respectively, i.e., the Fresnel reflection loss has been taken into consideration in the above equation.[23] The incident flux density used in Eqs. (6) and (9)–(11) can be obtained from this chart. As clearly seen, the optical flux decays exponentially for all the input light at 980 nm, 1310 nm, and 1550 nm. However, the decay is single-exponential for 980 nm but multi-exponential for 1310 nm and 1550 nm, which is mainly owing to that the absorption coefficient is not doping-dependent for 980 nm, i.e., the absorption coefficient is taken as a constant for all the active regions in this HPT;[24] however, as listed in Table 1, the absorption coefficients for 1310 nm and 1550 nm are layer-dependent, varying from layer to layer with different types and concentrations of doping.

The total current I_{total} of this HPT is the sum of the hole current at the base/depeted-collecter junction $I_{x=w_b}$, the electron current in the sub-collector region $I_{x=w_b+w_{dep}+w_c}$, and the current in the depleted-collector region I_{dr}. The responsivity can be obtained by I_{total}/P_{in}, where P_{in} is the incident light power. As shown in Fig. 3, the calculated responsivities for this $In_{0.53}Ga_{0.47}As$/InP HPT at 980 nm, 1310 nm, and 1550 nm are 6.34 A/W, 25.7 A/W, and 28.1 A/W, respectively, which are in good agreement with the measured values.

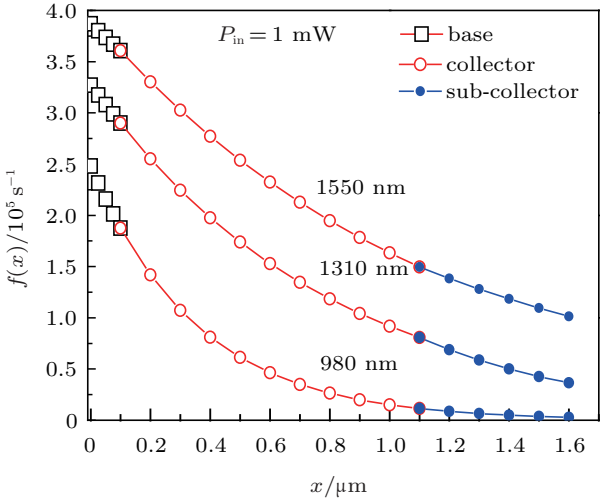


Fig. 2. (color online) The calculated optical-flux profiles for the $In_{0.53}Ga_{0.47}As$/InP HPT.

Table 1. Material parameters used for $In_{0.53}Ga_{0.47}As$/InP HPT simulation.

Parameter	Value	Unit	Reference
D_n, D_P	90, 6	$cm^2 \cdot s^{-1}$	[25]
τ_n, τ_p	4.3×10^{-9}, 4.3×10^{-9}	s	[26]
$L_n = (\tau_n D_n)^{1/2}$, $L_p = (\tau_p D_p)^{1/2}$	6.3×10^{-4}, 1.6×10^{-4}	cm	[22]
S_n, S_p	1×10^4, $\sim 10^6$	$cm \cdot s^{-1}$	[27]
$n_{p0} = n_i^2/N_A$, $p_{n0} = n_i^2/N_D$	2×10^4, 2×10^4	cm^{-3}	[28]
α_b(980 nm), α_b(1310 nm), α_b(1550 nm)	2.80×10^4, 1.20×10^4, 0.70×10^4	cm^{-1}	[23], [29]
α_{dep}(980 nm), α_{dep}(1310 nm), α_{dep}(1550 nm)	2.80×10^4, 1.28×10^4, 0.88×10^4	cm^{-1}	[23], [29]
α_c(980 nm), α_c(1310 nm), α_c(1550 nm)	2.80×10^4, 1.59×10^4, 0.78×10^4	cm^{-1}	[23], [29]

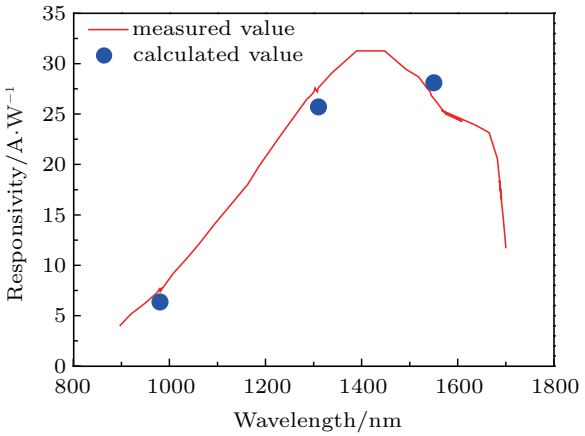


Fig. 3. (color online) Calculated and measured responsivities as a function of wavelength for the $In_{0.53}Ga_{0.47}As$/InP HPT.

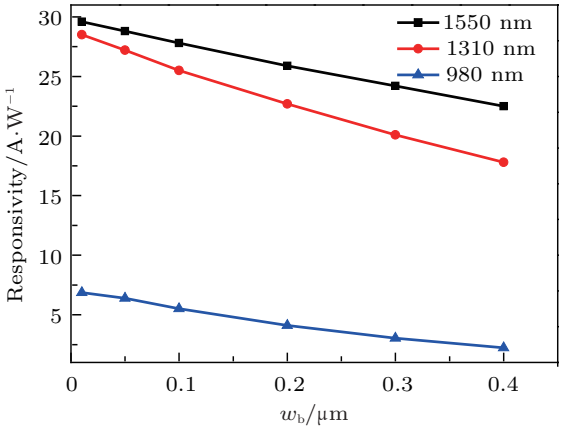


Fig. 4. (color online) Calculated responsivities versus the base width for the $In_{0.53}Ga_{0.47}As$/InP HPT at various incident wavelengths.

We assume that the InP substrate and the emitter region are transparent to NIR light, i.e., light absorption starts from the base layer. For a constant incident light power, the optical flux increases with the increase of the wavelength, resulting in increasing photo-generated electron–hole pairs. While the absorption coefficient is opposite, thus, leading to a responsivity peak at about 1420 nm, and the responsivity tends to drop at longer wavelengths owing to the lower absorption coefficient, which causes a cut-off wavelength around 1700 nm.

For various base widths, the corresponding responsivities are shown in Fig. 4. As observed in this figure, the responsivity has a near linear falling with the increase of the base width. It is common knowledge that an increase in the base width is related to an increasing recombination of the minority-carrier holes and the majority-carrier electrons in the base region, which will lead to a decreasing built-in current gain, i.e., a decreasing responsivity. However, different decreasing rates in responsivity can be found for the under-investigated $In_{0.53}Ga_{0.47}As$/InP HPT at 980 nm, 1310 nm, and 1550 nm due to the different absorption coefficients and optical-flux profiles in the base region. For the incident light of the wavelength of 1310 nm, the absorption coefficient is lower compared to that of 980 nm, and the optical flux is fewer compared to that of 1550 nm, leading to the fewest photo-generated carriers compared to those at 980 nm and 1550 nm, hence, the falling rate is highest at 1310 nm.

5. Conclusion

An accurate spectral response model for the back-illuminated p–n–p $In_{0.53}Ga_{0.47}As$/InP HPT has been established by applying the semiconductor continuity equations with the exacted boundary conditions which contain the thermal equilibrium minority-carrier electrons (holes). Twice Fresnel reflection and the diffusion current of the electrons from the sub-collector have been taken into consideration in this model. The calculated responsivity is close to the measured one, which has a peak at about 1420 nm. Furthermore, a nearly proportional relationship between the responsivity and the base width has been found in this work.

References

[1] Walker D, Monroy E, Kung P, Wu J, Hamilton M, Sanchez F J, Diaz J and Razeghi M 1999 *Appl. Phys. Lett.* **74** 762
[2] Zhou J J, Jiang R L, Sha J, Liu J, Shen B, Zhang R and Zheng Y D 2003 *Chin. Phys. B* **12** 0785
[3] Li C, Xue C L, Liu Z, Cheng B W, Li C B and Wang Q M 2014 *Chin. Phys. B* **23** 038506
[4] Zhang Y, Shen S C, Kim H J, Choi S, Ryou J H, Dupuis R D and Narayan B 2009 *Appl. Phys. Lett.* **94** 221109
[5] Li X J, Zhao D G, Jiang D S, Liu Z S, Chen P, Wu L L, Li L, Le L C, Yang J, He X G, Wang H, Zhu J J, Zhang S M, Zhang B S and Yang H 2014 *Chin. Phys. B* **23** 028503
[6] Kamitsuna H 1995 *J. Lightw. Technol.* **13** 2301
[7] Lunardi Y C, Chandrasekhar S and Hamn R A 1993 *IEEE Electron Device Lett.* **14** 19
[8] Cappelletti M A, Cedola A P, Peltzer E L and Blanc Y 2009 *Semicond. Sci. Technol.* **24** 105023

[9] Cuevas J A R G, Abedin T F, Ali M N E and Hani E 2006 *Opt. Eng.* **45** 044001
[10] Arnold M S, Zimmerman J D, Renshaw C K, Xu X, Lunt R R, Austin C M and Forrest S R 2009 *Nano Lett.* **9** 3354
[11] Chand N, Houston P A and Robson P N 1985 *IEEE Trans. Electron Devices* **ED-32** 622
[12] Salles A A D, Hackbart A S and Spalding L N 1994 *Microw. Opt. Technol. Lett.* **7** 392
[13] Frimel S M and Roenker K P 1997 *J. Appl. Phys.* **82** 3581
[14] Sridhara R, Frimel S M, Roenker K P, Pan N and Elliott J 1998 *J. Lightw. Technol.* **16** 1101
[15] Khan H A, Rezazadeh A A, Sohaib S and Tauqeer T 2012 *IEEE J. Quantum Electron* **48** 576
[16] Chen J, Ban D, Helander M G, Lu Z, Graf M, Poole P and Liu H C 2009 *IEEE Photonics Technol. Lett.* **21** 1447
[17] Chen J, Ban D, Helander M G, Lu Z H and Poole P 2010 *Adv. Mater.* **22** 4900
[18] Tseng H C 2007 *IEEE Adv. Packag. Trans.* **30** 823
[19] Mashade M B E, Ashryb M, Eladl S M and Rageh M S 2004 *Microelectron. J.* **35** 585
[20] Khan H A, Rezazadeh A A and Saleem R 2012 *Jpn. J. Appl. Phys.* **51** 072202
[21] Khan H A and Rezazadeh A A 2009 *IEEE Electron Device Lett.* **30** 1158
[22] Sze S M 1981 *Physics of Semiconductor Devices* (2nd Edn.) (New York: Wiley)
[23] Bashar S A 1998 *Study of Indium Tin Oxide (ITO) for Novel Optoelectronic Devices* (Ph.D. Dissertation) (London: King's College London)
[24] Broberg B and Lindgren S 1984 *J. Appl. Phys.* **55** 3376
[25] Sheng H 2000 *Modelling, Fabrication and Characterisation of InP-HBTs for Future High-speed, Low power Optical Telecommunications* (Ph.D. Dissertation) (London: King's College London)
[26] Ahrenkiel R K, Ellingson R, Johnston S and Wanlass M 1998 *Appl. Phys. Lett.* **72** 3470
[27] Tonai I 1991 U.S. Patent 5053837 [1991-10-1]
[28] Tyagi M S 2008 *Introduction to Semiconductor Materials and Devices* (New York: John Wiley & Sons)
[29] Humphreys D A, King R J, Jenkins D and Moseley A J 1985 *Electron. Lett.* **21** 1187